Modeling volcanic deformation in a regional stress field: Implications for the formation of graben structures on Alba Patera, Mars

Beatrice Cailleau,[1] Thomas R. Walter,[2] Peter Janle,[3] and Ernst Hauber[4]

Received 12 June 2003; revised 20 October 2003; accepted 30 October 2003; published 30 December 2003.

[1] Abundant grabens transect the volcano Alba Patera. Their complex geometry and formation mechanisms are still poorly understood. Tectonic processes and magmatic intrusions are responsible for these long surface features. Cross-cutting relationships of the grabens show radial fractures that were formed during early stages and were progressively overprinted by concentric fractures on the mid and upper flanks of the volcano. Two modeling methods are used to understand the formation of the observed structures and to evaluate their implications for hidden subvolcanic processes. Surface deformation and fault arrangements predicted in finite element models are compared to the graben systems observed in Viking images. The orientation and position of the concentric grabens are found to be best reproduced by local crustal subsidence, superimposed on a regional NW-SE oriented extension with decreasing magnitude from south to north. In analogue sandbox models we also simulate surface structures of arrangements that almost perfectly mimic the observed lineaments on Alba Patera. Formation of the grabens spans a period on the order of a billion years, suggesting long-term geodynamic processes to be responsible for the subsidence of the central Alba Patera area. The progressive change toward higher concentricity is likely resultant from an increase in density in the crust by accumulation of intrusive material and cooling, thus causing subsidence of the region above this volcanic root. *INDEX TERMS:* 5480 Planetology: Solid Surface Planets: Volcanism (8450); 6225 Planetology: Solar System Objects: Mars; 8149 Tectonophysics: Planetary tectonics (5475); 8120 Tectonophysics: Dynamics of lithosphere and mantle—general; 8164 Tectonophysics: Stresses—crust and lithosphere; *KEYWORDS:* Alba Patera, Mars tectonics, volcano deformation, doming and subsidence, dike intrusion

Citation: Cailleau, B., T. R. Walter, P. Janle, and E. Hauber, Modeling volcanic deformation in a regional stress field: Implications for the formation of graben structures on Alba Patera, Mars, *J. Geophys. Res.*, *108*(E12), 5141, doi:10.1029/2003JE002135, 2003.

1. Introduction

[2] The Tharsis volcanic region is an 8000 km wide dome characterized by giant grabens that extend radially from the center and become arcuate at the periphery (Figure 1a). The formation and orientation of these extensive grabens were explained by tectonic models in which the gravitational load of the volcanic region induces isostatic stresses, flexural bending stresses and/or membrane stresses and subsequent deformation [e.g., *Turcotte et al.*, 1981; *Sleep and Phillips*, 1985; *Tanaka et al.*, 1991; *Banerdt et al.*, 1992; *Banerdt and Golombek*, 2000]. Since extensive grabens are probably the surface expression of giant dikes, magmatic processes were proposed [e.g., *Mège and Masson*, 1996; *Wilson and Head*, 2002]. Doming above a plume or a wide deep reservoir in a regional stress field could account for radial to arcuate giant dike swarms (Figure 1a).

[3] At the northern periphery of Tharsis, Alba Patera is one of the most peculiar and widespread volcanoes known in the planetary system, measuring up to 2700 km across and 7 km in height (Figure 1b). The edifice is characterized by numerous extensional fractures in a predominantly north-south direction that curve around the summit, implying combined influences of regional and local stress fields. The grabens are up to 1000 km long, and have a width which is on the order of 2–10 km, with common depths between 100 and 350 m [*Gibbons et al.*, 2001; *Scott et al.*, 2002]. The same authors estimated the dike thicknesses underlying the grabens around Alba Patera between 150 and ~700 m, with dike top depth up to 4 km. Graben formation on Alba Patera was active (and reactive) from Noachian to Late Amazonian. We use the relative age relationships proposed by *Tanaka* [1990] reproduced in Figure 2. South of Alba Patera, the faulting of the Ceraunius Fossae began in phase I in the Noachian epoch and pursued until the early Amazonian. The main faulting of the Ceraunius Fossae is oriented north-south, radial to Tharsis (Figure 1). During the phase II, widespread volcanism of Alba Patera started,

[1]GEOMAR, Kiel, Germany.
[2]Marine Geology and Geophysics, Rosenstiel School of Marine and Atmospheric Science, Miami, Florida, USA.
[3]Institute of Geosciences, Department of Geophysics, Kiel University, Kiel, Germany.
[4]Institut für Planetenforschung, Deutsches Zentrum für Luft- und Raumfahrt (DLR), Berlin, Germany.

0148-0227/03/2003JE002135

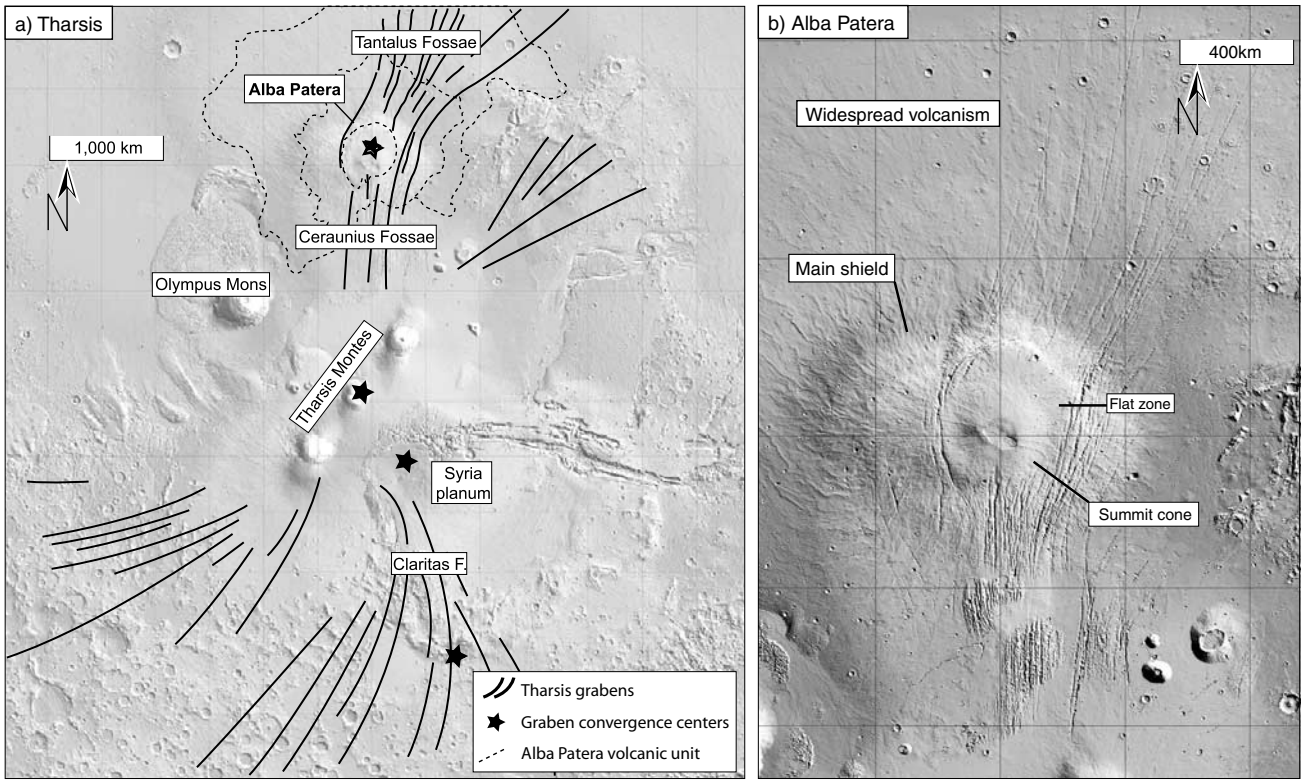

Figure 1. a) Regional setting of Alba Patera. The Tharsis region is characterized by giant grabens radial to the Tharsis center and arcuate at the periphery. The Ceraunius Fossae to the south of Alba Patera and radial to Tharsis are linked to the Tharsis or Syria Planum centers. The concentric structures and the Tantalus Fossae radial to Alba Patera indicate an autonomous magmatic center under the volcano, though they are influenced by the regional field [*Mège and Masson*, 1996]. The dotted contours illustrate the extent of the 3 main volcanic units of Alba Patera after *Scott and Tanaka* [1986]. b) MOLA 0.125° shaded relief of Alba Patera showing the topographic characteristics of the three volcanic units. There is a change from widespread to centralized volcanism with increasing slope between each unit. The main shield has an E-W diameter of 1300 km, a N-S diameter of about 600 km and a height of 5 km. It is topped by a flat zone that is 1 km higher on the western flank than on the eastern side. The summit cone surrounded by concentric grabens and the flat zone is 400 km across and 2 km high.

fractured by the northeast trending Tantalus Fossae (Figure 1). In phase III, centralized volcanism gave rise to the main shield, 1300 km in diameter and 5 km in height and numerous grabens formed on the upper and mid-flanks of the main shield (Figure 1b and Figure 3). The final stage of phase III is characterized by the construction of the summit cone, 400 km wide and 2 km high, on the top of the main shield, the formation of fine highly concentric fissures (Figure 4a) and the radial wrinkle ridges and the calderas.

[4] On the basis of cross-cutting relationships and the orientation of the grabens observed on Viking images, we are able to define the tectonic evolution of phase III, the focus of our study. Radial structures on the main shield of phase III are probably the result of continuous faulting or reactivation of faults from phase II. New fractures appear in a concentric fashion transecting the northeast grabens on the north western and eastern flanks (Figures 4b and 4c). The concentric structures formed after radial faulting and mostly before the summit cone. Only a few of these grabens cut lava flows from the late edifice. Continuity of concentric structures with radial grabens is observed to the south in the Ceraunius Fossae and to the northeast in the Tantalus Fossae (Figure 4d), suggesting a progressive change from a radial to a concentric pattern. The Catenae are grabens with pit craters originated from the Tharsis activity [*Tanaka*, 1990; *Mège and Masson*, 1996]. The eastern Catenae are likely to be contemporaneous with the radial Tantalus Fossae because their fault trend is similar and the Catenae are cross-cut by the concentric Tantalus Fossae (Figure 4b). Reactivation of the eastern Catenae occurred in a phase IV during middle-late Amazonian epoch [*Tanaka*, 1990]. The western Catenae comparable in orientation with the concentric Alba Fossae were probably influenced by the same stress field, thus at similar epoch in the late stages of the Alba Patera tectonics. Considering the entire edifice, Alba Patera was subjected to an extremely long period of graben growth (Figure 2). The orientations of the tectonic structures overall tend toward stronger concentricity still after the summit cone formation (e.g., see SW flank of summit cone, Figure 4a).

[5] Until Mars Global Surveyor (MGS) was launched in 1996, the topographic characteristics of Alba Patera were poorly constrained. The concentric lineaments were located

Epoch		*Orientation*	*Tectonics*	*Volcanism*	*Age*
Early Amazonian	III	Concentric	Calderas - Ridges Tantalus Fossae Alba Fossae Western Catenae	Summit cone Main shield	2.9 -2.1 by
Late Hesperian		Radial	Tantalus Fossae Ceraunius Fossae	Main shield	3.6 3.1by
Early Hesperian	II	Radial, north-east	Tantalus Fossae Eastern Catenae	Tantalus unit Widespread	3.7 - 3.6 by
Late Noachian		Radial, north-south	Ceraunius Fossae	Ceraunius volcanic units	3.8 - 3.7 by
Middle Noachian	I				3.92 - 3.8 by
Early Noachian					Before 3.92 by

1.8 by

Figure 2. Tectonic and magmatic evolution of Alba Patera. Modified after *Tanaka*'s [1990] study based on crater counts, fault stages and geologic units. The ages for the epochs are after *Hartman and Neukum* [2001]. Structures and volcanic units are sketched in Figures 3 and 4. This study focuses on the faulting of phase III.

at the foot of the main shield, at that time consistent with the flexural deformation of the lithosphere under the volcanic load [*Wise*, 1976; *Comer et al.*, 1985; *Turtle and Melosh*, 1997; *Heller and Janle*, 2000]. Location derived by MGS at much higher elevation on the flanks of the edifice requires additional processes (Figure 1b). *McGovern et al.* [2001] proposed that concentric normal faulting may arise from uplift by sill complexes combined with a growing surface loading. With this model, McGovern and co-authors could reproduce the morphology of the volcano with a flat zone separating the steep summit cone to the underlying main shield in a single process. However, the younger age of the summit volcanic unit derived from crater counts [*Scott and Tanaka*, 1986] probably implies a different genesis. *Scott and Wilson* [2003] suggested that the fractures resulted from crustal subsidence and spreading after the rebound due to the detachment of Alba Patera's root. This process would induce compressive structures at the margin of the volcano which are however not observed [*Scott and Wilson*, 2003]. Although several studies have been devoted to understand the concentric fractures on Alba Patera, no consensus has been found yet.

[6] We propose a new evolutionary model based on rifting and intrusive processes. The goal is to better understand the transition from radial grabens in pre- or early stages of Alba Patera to concentric orientation and to determine the processes responsible for the geometric characteristics of the tectonic structures (Figure 3). The deformation and stress fields induced by subsidence together with a regional extension are reconstructed in finite element and analogue models. The two methods give similar and complementary results, so that the effects of the main forces, i.e., subsidence, regional stress and surface loading, and their interactions can be outlined with confidence. From these models and observed surface features we develop an idea of the deep volcanic and crustal structure. Comparison of these theoretical cases with Alba Patera and similar structures known on Earth provides additional information on the geodynamic processes that prevailed on the Martian volcano.

2. Numerical Models

[7] Deformation of Alba Patera exerted by magmatic and gravitational forces are numerically simulated to estimate the surface displacements and stress fields. We use the Finite Element program TEKTON [*Melosh and Raefsky*, 1983]. First, we simulate stress fields that arise from local volcano-tectonic processes. The stress field and corresponding regions of faulting are presented for two types of subsidence, either due to a higher density core within the volcano or due to the topographic load. We describe the effect of varying the dimensions and depth of an intrusive core (or a reservoir). We show how the surface stresses caused by the local subsidence interact with the topographic loading. Second, the local deformations are combined with the regional extension of E-W and NW-SE orientations.

2.1. Finite Element Method

2.1.1. Model Geometry and Material Characteristics

[8] An elastic half-space is used to estimate the response of the crust to subsurface loading (Figure 5). The density of the crustal rock is taken to be 2900 kg/m^3 [*Zuber*, 2001], Young's Modulus to be 50 GPa and Poisson's ratio to be 0.25 [*Turcotte and Schubert*, 1982]. Gravitational acceleration on the Mars surface is 3.7067 m/s^2. When specified, the topography of Alba Patera is considered. The volcano's dimensions are 650 km in radius and 5 km in height. In order to speed up processing time and model construction, we use a cosine form to reproduce the approximate shape of the edifice.

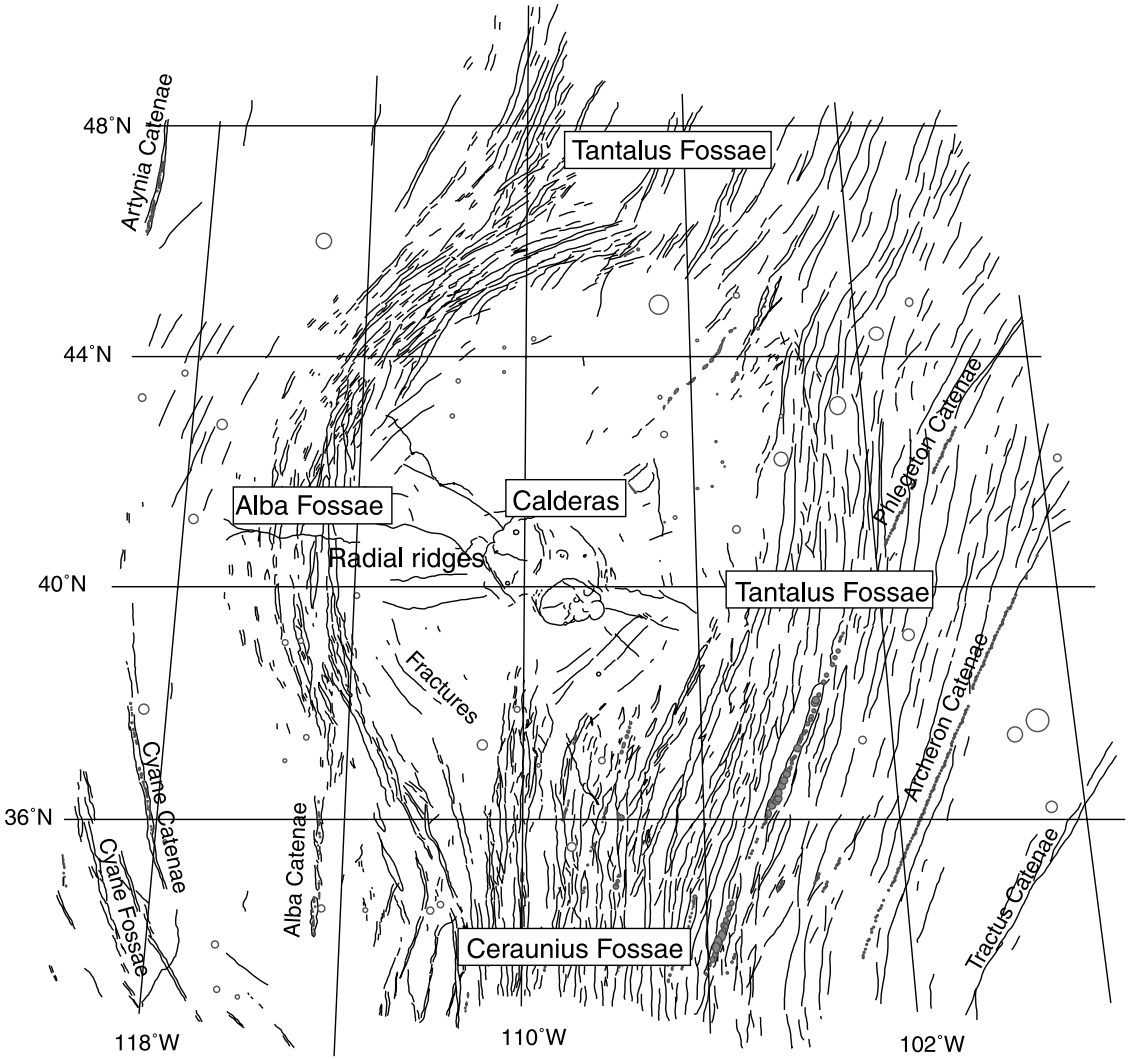

Figure 3. Tectonics on the main shield and summit cone of Alba Patera. This map has been constructed from a Viking mosaic with a resolution of about 60 m/pixel. This illustrates the geometric characteristics of Alba Patera tectonics which will be reconstructed by numerical and analogue modeling in this study. Alba Patera's set of grabens has a typical wrist-watch shape. The trend of the faulting is concentric on the eastern and western flanks and changes progressively toward the radial pattern to the north and south. To the northwestern side, however, the Alba Fossae display a high concentricity and cross-cut the northeast radial Tantalus Fossae. The two sets of concentric fractures are asymmetric. The Alba Fossae are clearly concentric and restricted to a 100 km wide zone. In contrast, the Tantalus Fossae are north-south slightly concentric near the summit and tend toward a NE-SW linear pattern on the lower flanks. The eastern grabens are numerous, observed down to the middle-lower flanks. The Catenae are grabens with pit craters related to regional dikes [*Mège and Masson*, 1996]. The eastern Catenae follow the regional Tharsis trend (Figure 1a) while the concentric western Catenae were probably influenced by a stress field local to Alba Patera. The radial ridges on the summit cone are thought to be compressive in nature. There are twice as many branches of ridges on the western side than on the eastern side and the whole set of ridges is NW-SE oriented.

[9] Subsurface loading is simulated by changes of density at depth relative to the surrounding rocks (Figure 5). The region of density difference within the crust is modeled elliptically in form and is termed for simplification the volcanic "core." The physical meaning of this region, i.e., plume, underplating, magma chamber or intrusive complex, can be determined a posteriori from the characteristics of the model that best correlate with the observed structures. A higher density simulates any crustal subsidence, e.g., cooling magma, decrease of preexisting support or change of crustal strength. The models of subsidence best reproduce the concentric grabens of Alba Patera.

[10] Figure 5 illustrates part of the finite element mesh and the boundary conditions. The bottom and lateral sides are far enough to avoid boundary effects. The element size is larger at high horizontal and vertical distances of the

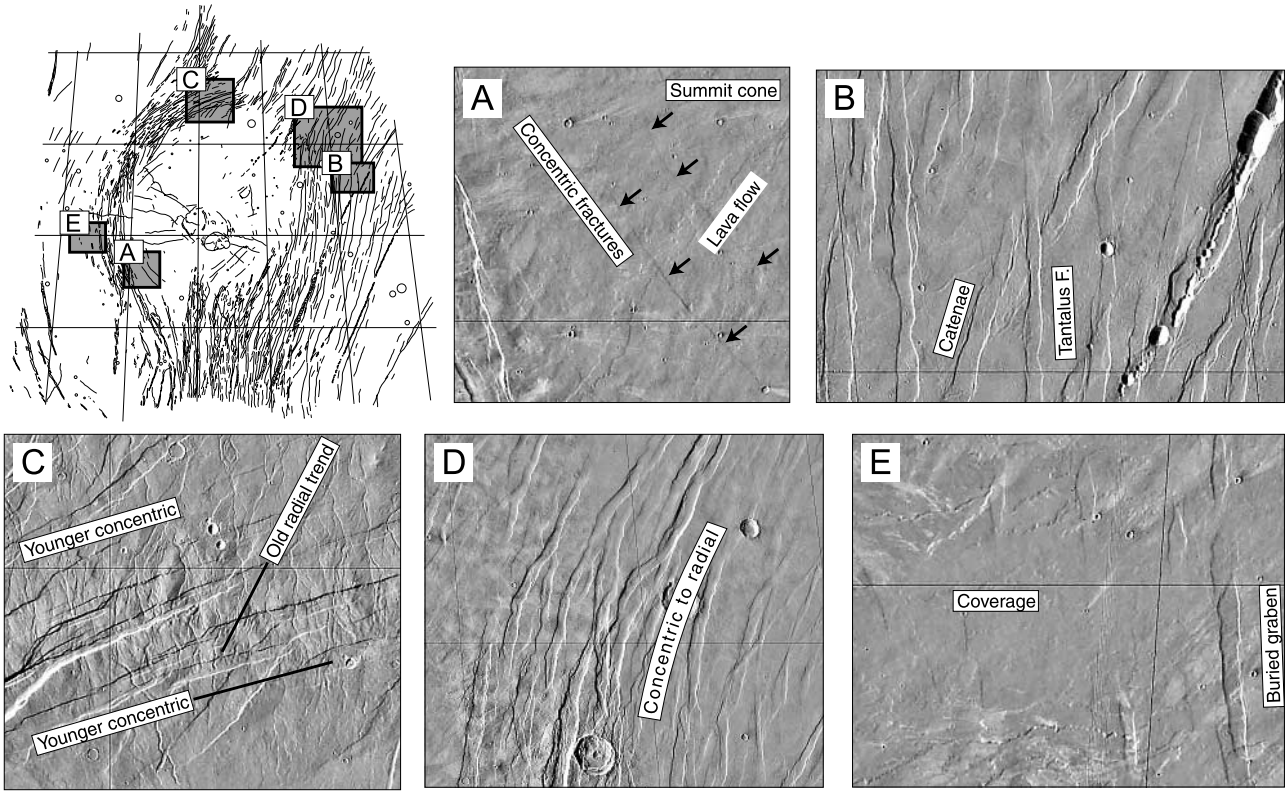

Figure 4. Details of Viking image mosaic (resolution of ~60 m/pixel, orbits 252S to 254S). A) Fine fractures at the base of the summit cone do not modify the trend of a lava flow from the summit. The fractures are therefore younger, indicating that new circumferential fracturing occurred late in Alba Patera's history. B) The Catenae are cross-cut, i.e., postdated, by the concentric Tantalus Fossae. C) Second example of cross-cutting by concentric grabens. The concentric fracturing occurred after radial faulting on Alba Patera. Grabens postdate an intense erosion stage, this area being highly eroded by meandering channels thought to be caused by sapping in an upper ash layer [*Mouginis-Mark et al.*, 1988]. D) Continuity is also observed between concentric and radial faults, here for the case of the Tantalus Fossae to the northeastern side. E) On the western side, grabens were covered by ash or lava flows.

studied area to limit the number of elements and processing time. The model is axisymmetric so that only half of the grid needs to be meshed. There is no horizontal displacement at the axis of symmetry and on the far vertical side. These two boundaries are free to move vertically. The bottom of the grid is fixed.

2.1.2. Modeling Procedures

[11] Finite Element program TEKTON resolves the equation [KU = P] where U is the vector of unknown displacements. The K matrix depends on Young's Modulus and Poisson's ratio, and on the geometry of the elements, here axisymmetric quadratic elements. P is the vector of applied forces and in this model represents the gravitational load, i.e., the body forces, depending on gravity g and density ρ. The FE program calculates the displacements and the stress tensors.

[12] The model is no longer axisymmetric when a regional stress is added. The axisymmetric stress tensor (σ_{rr}, $\sigma_{\theta\theta}$, $\sigma_{r\theta}$) is thus transformed into (σ_{xx}, σ_{yy}, σ_{xy}) in a Cartesian coordinate system by the means of a Mohr diagram. For a detailed description of stress transformations, the reader is referred to *Twiss and Moores* [1992]. Two types of regional stresses are tested: an E-W extension of constant magnitude over the Alba Patera area and a NW-SE extension whose magnitude decreases in a cosine form from 40° latitude to 60° latitude. σ'_{xx}, σ'_{yy}, σ'_{xy} are the stresses resulting from combining the local stresses determined using TEKTON and the regional stresses.

[13] To compare the numerical models to the observed grabens on Alba Patera, we need the maximum and minimum principal stresses σ_1 and σ_3, respectively. These are calculated from the precedent stresses (σ_{xx}, σ_{yy}, σ_{xy}) or (σ'_{xx}, σ'_{yy}, σ'_{xy}) by using the program TEKTON. Fracture experiments have shown that the initiation of fracturing depends on the differential stress ($\sigma_1 - \sigma_3$) [e.g., *Twiss and Moores*, 1992]. Alternatively, the fractures near the surface may simply depend on the maximum tensile stress. The direction of σ_1 gives the orientation of fractures or dikes. The different regions of faulting predicted are determined using *Anderson*'s [1951] theory, which is modified to suit the convention of a positive stress for extension. Theoretically, it is expected that a) thrust faults form when the minimum compressive stress σ_3 is vertical, b) normal faults when the maximum compressive stress σ_1 is vertical, c) strike-slip faulting when the vertical principal stress is intermediate. In order to superpose the numerical models to the mosaics of Alba Patera, the coordinates (X, Y) in meters are transformed to degrees and from an

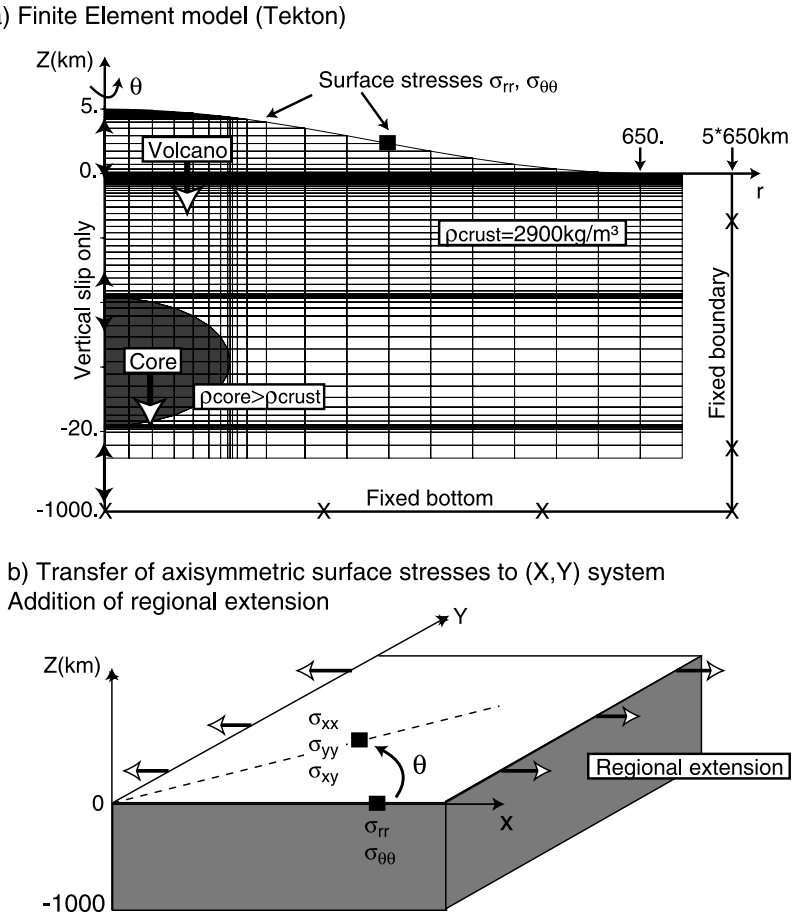

Figure 5. Axisymmetric model of topographic loading and subvolcanic core. The source of deep forces is unknown and ideally modeled by an elliptic area that has a density different from the surrounding rock. A higher density simulates any crustal subsidence by cooling, withdrawal of magma or dying support from below. The boundary conditions are indicated. For a better illustration of the mesh, we significantly reduce the vertical size of the core and the number of elements and exaggerate the vertical scale in regards to the horizontal axis. Alba Patera is an extremely flat volcano with less than 1° slope. The effects of regional extension are also tested. The axisymmetric stresses of surface or subsurface loading must be projected onto an (X, Y) system before addition of regional extension by means of a Mohr diagram.

aerocentric to an aerographic system (the planetographic system).

2.2. Subsidence Due to the Volcanic Core or the Topographic Loading

[14] Two types of faulting are predicted on the surface for a shrinking volcanic core. Compression involving thrust faults is expected along a radial distance similar to the horizontal radius of the reservoir (Figure 6a). Around the distal edge of the reservoir, there is a high tensile radial component generally associated with compressive hoop stress leading to strike-slip faulting. Similarly, crustal subsidence can be created by the topographic load. Variations of stresses induced by the topography alone are thus comparable to the previously described effect of subsidence (Figure 6b). For both types of subsidence, a third region of concentric normal faulting encircling the strike-slip faulting area is expected because the compressive hoop stress is low relative to the radial tensile stress. Since the minimum stress level for normal failure is approximately a half of that required for strike-slip faulting [*Weijmars*, 1997], only normal faults will form and no strike-slip faults and may be true in the whole immediate surrounding of the volcano in case of topographic loading or above the distal edge of a shrinking core. The maximum stresses for topographic loading are situated at the foot of the volcano and can not account for the concentric grabens on the upper and middle flanks of Alba Patera. This could be better explained by the subsidence or contraction of a volcanic core. The characteristics of the core remain undetermined.

2.3. Variations of Core Characteristics

[15] The effects of varying the core characteristics are shown in Figure 7. Widening the horizontal or the vertical size of the core, and/or increasing its depth enlarges the regions of faulting on the free surface. Higher density difference between the core and surrounding rocks augments the magnitude of the stresses. This does not modify, however, the horizontal extent of the deformation on the surface. Greater stresses are also obtained for shallower intrusive cores. The surface stresses for a wider reservoir are larger, because its upper walls are closer to the surface. The

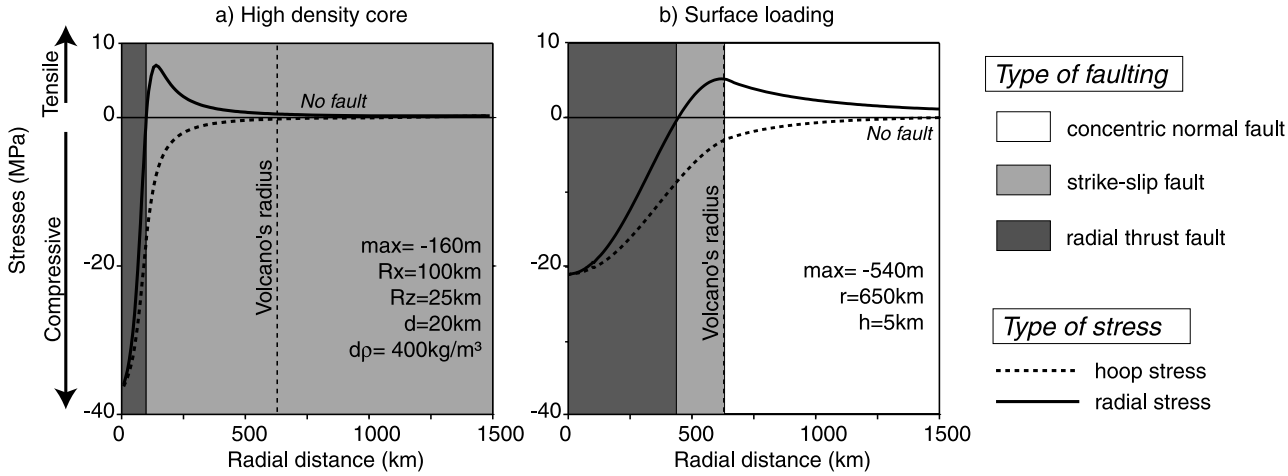

Figure 6. Axisymmetric surface stresses and corresponding types of faulting after *Anderson*'s [1951] theory for two types of subsidence: a) a volcanic core of higher density relative to the surrounding rock and b) surface loading. Positive stresses are tensile. The horizontal and vertical radii of the reservoir are Rx and Rz, d is the depth to its top, dρ the difference of density relative to the surroundings. The radius of the volcano is r, the height is h. "max" is the maximum value of displacements observed in all cases at the axis of symmetry. When the tensile radial stresses are much higher than the compressive hoop stresses, normal faulting is more likely (here indicated for the case of surface loading).

geometric link between the observed fractures and the size and position of the core allows us to estimate the dimensions and depth of the core.

[16] The position of maximum tensile stresses is studied for various depths and radii of the core (Figure 8). As seen in Viking images, the concentric fractures are most pronounced at 200–300 km from the volcano summit. In principle, to obtain this position in numerical models between 200 and 300 km radial distances from the axis of symmetry, the horizontal radius of a shrinking core

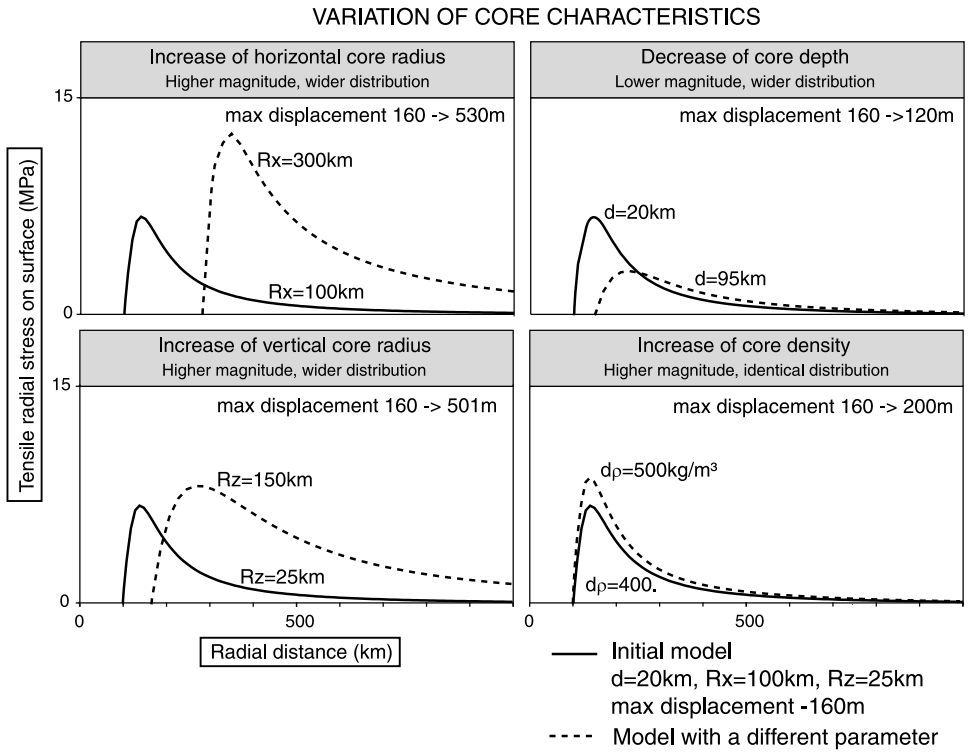

Figure 7. Tensile radial stresses on the surface for the variation of size, depth and density of the core. The model of subsiding core of Figure 6a is the initial model. In each case, we vary only one parameter at a time. The variation of maximum downward displacements found at the axis of symmetry or summit is shown in meters.

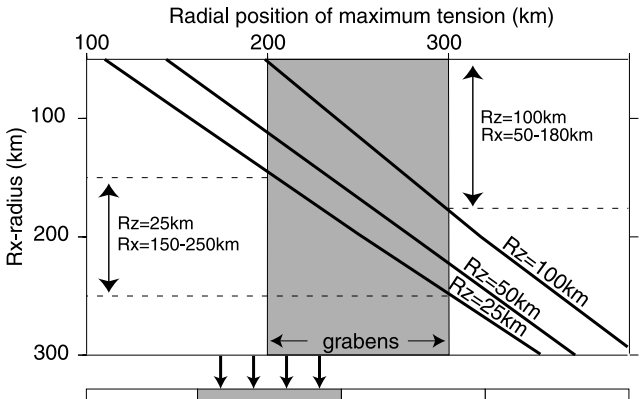

Depth d	d= -30km	d= -50km	d= -80km
Rz=100km	Rx=50-180km	Rx=50-160km	Rx=50-120km
Rz=50km	Rx=120-220km	Rx=90-200km	Rx=120-170km
Rz=25km	Rx=150-250km	Rx=130-230km	Rx=90-200km

Figure 8. Ranges of dimensions of the subsiding core that lead to maximum tensile stresses between 200 and 300 km away from the axis of symmetry or summit (the gray shaded area). This corresponds to the radial distances of the more pronounced concentric fractures on Alba Patera. The plot above presents the method for constraining the dimensions of the core for a 30 km depth, d, to the top of the core. The horizontal and vertical radii, Rx and Rz, respectively, are varied and the radial position of the corresponding maximum tension is plotted. The table below contains the dimensions of the core(s) that give correlations between the position of maximum tension and the position of concentric fractures between 200 and 300 km radial distances. Three different depths to the top of the core are tested. The solutions are multiple. Increasing the depth and/or the vertical radius results in decreasing the horizontal radius of the core to obtain correlation.

must be in the range of 150–250 km, if its vertical radius is low (<25 km) and if the top of the core is at 30 km depth. The core is then oblong, similar to a sill complex. For a deeper core, at 50 and 80 km depth, the horizontal radius must be shorter by 20–50 km. For a long vertical radius of 50–100 km, the horizontal radius must be relatively small, i.e., the core needs to have a more circular shape to obtain similar regions of deformation on the surface. This illustrates the non-uniqueness of solutions for the shape and depth of the subsurface load for this type of model.

2.4. Combination of Core Subsidence With Surface Loading

[17] The influence of the volcanic load is combined with the models described above. Around the summit, the subsidence of the volcanic core augments the compression due to the surface loading (Figure 9). A subsiding core of small extent relative to the size of the volcano and of realistic magnitude has its tensile effect swept out by the compression induced by the volcano. Thus concentric grabens on the upper and mid-flanks of the volcano are unlikely to form. Subsidence of a larger extent increases the tension at the base of the volcano. For a subsiding core of 300 km horizontal radius and 25 km vertical radius, at 20 km depth from the surface to the top of the core, the tension affects all of the mid to lower flanks. These last results, however, disagree with the absence of concentric grabens at the foot of the volcano. The stresses due to the volcano's load, either tensile or compressive, must be low to produce fractures on the upper and middle flanks. Therefore we now test the hypothesis of whether a regional stress was jointly involved. A potential source of this stress field is the Tharsis dome to the south.

2.5. E-W Regional Stress Combined With Subsiding Core or Topographic Loading

[18] In this section, we combine the effects of a regional east-west extension with the above mechanisms of subsidence. Thanks to symmetry in the problem, only a quarter of the surface is plotted. Figure 10a is the combined result of two distinct numerical models. On the left-hand side, the effect of only the local forces is presented. On the right-hand side, the local forces are combined with a regional

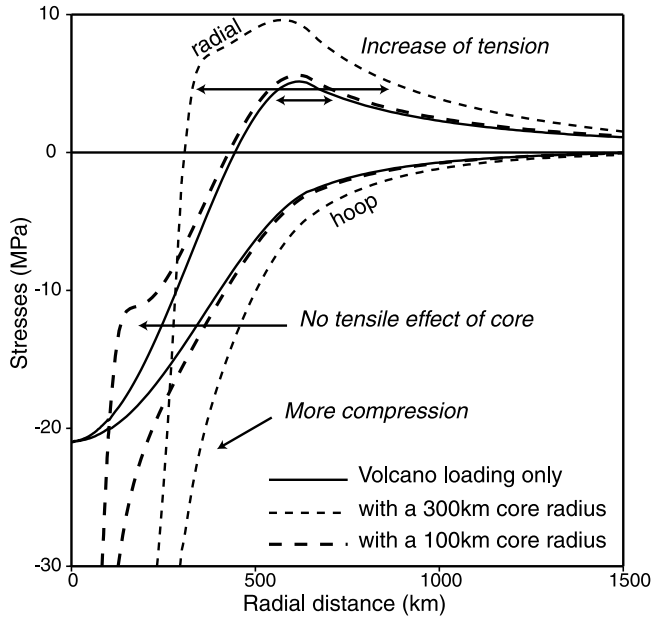

Figure 9. Combination of a subsiding core with volcano loading. The volcano has a radius of 650 km and a height of 5 km. Subsidence due to the core is simulated by a density increase of 400 kg/m^3 in an elliptic area of 300 km or 100 km horizontal radius and fixed vertical radius of 25 km. The depth to the top of the core is 20 km. In the three cases, the radial stress is greater than the hoop stress, as indicated for a 300 km core radius. A subsiding core induces compression near the axis of symmetry and tension at a radial distance corresponding to the radius of the core (Figure 6a). A subsiding core augments the compression due to surface loading near the axis of symmetry and augments the tension due to surface loading at the foot of the volcano. A core of small radius, e.g., 100 km, has its tensile effect deleted by the high compression of the surface loading. Thus combined surface loading and a subsiding core cannot create grabens on the upper and mid-flanks of the volcano as observed on Alba Patera.

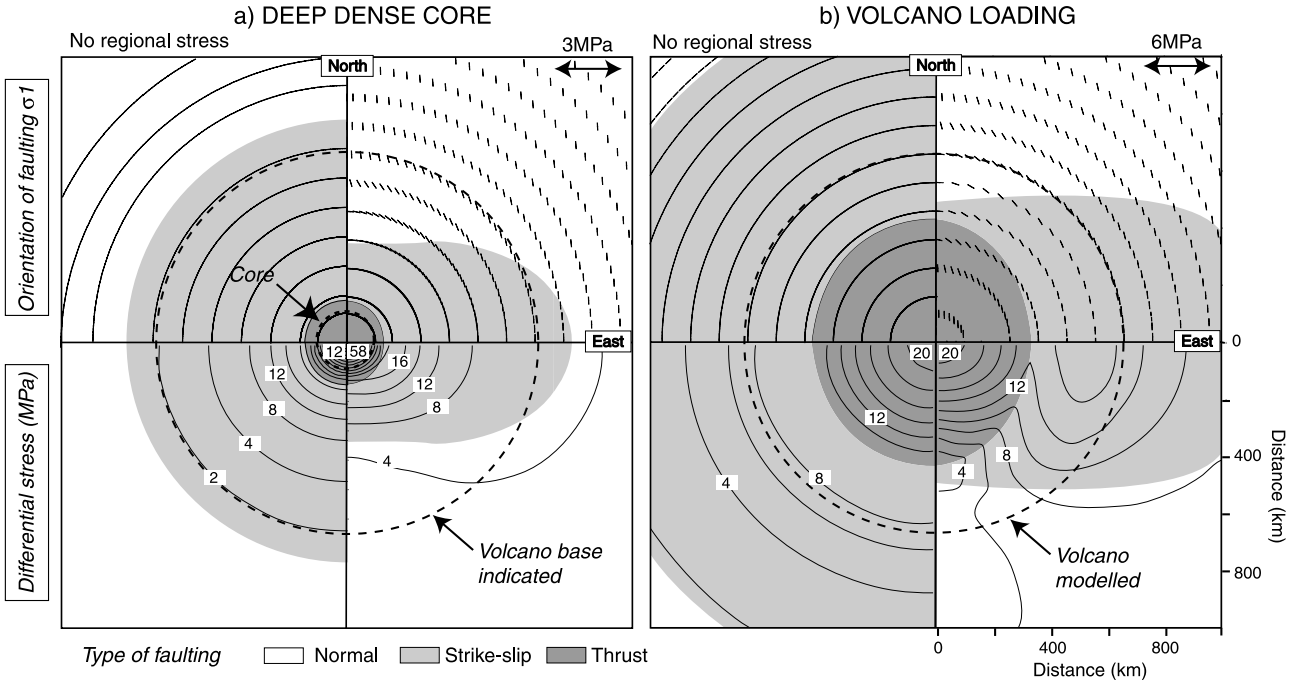

Figure 10. Type and orientation of faulting for a combination of an east-west regional stress with two types of subsidence. a) Subsiding core (left) and combination with regional stress (right). Subsidence is simulated by a density increase of 300 kg/m^3 relative to the surrounding in a circular core of 100 km radius at 30 km depth to its top. b) Volcanic loading (left) and combination with regional stress (right). The volcano has a height of 5 km and a radius of 650 km. In both cases of subsidence, the predicted types of faulting on the free surface are normal faults (white), strike-slip faults (gray), and thrust faults (black) after *Anderson*'s [1951] theory. On the top, the orientations of the maximum compressive stress σ_1 giving the orientation of normal faulting are presented. Thrust faults arising from compression (black area) are perpendicular to σ_1. At the bottom, the contours of differential stress ($\sigma_1-\sigma_3$) are shown. Maximum differential stress gives the position of likely failure. The dashed circle indicates the contour of a volcano 1300 km across.

extension. Where the regional stress is dominant in an E-W rifting environment, the orientation of likely faulting or dyke propagation is north-south, perpendicular to the least compressive stress direction. Thus regional stress can contribute solely to the N-S directed grabens on Alba Patera. If the root of Alba Patera contracts or subsides slightly, concentric fractures can form on the flanks of the volcano. Regional stresses added to local subsidence give rise to a typical form of faulting. This model predicts a change from concentric structures near the summit of the volcano to linear or radial patterns at the lower flanks and surroundings; similar structures on Earth are termed "wristwatch" shape [*van Wyk de Vries and Matela*, 1998] (Figures 10a and 10b).

[19] Without a regional stress, the differential stress is axisymmetric (left-hand side, Figure 10a). With addition of an east-west regional extension, the lines of equal differential stress are no longer concentric, so that fractures may not contour the whole volcano. For example, the differential stresses for a combination of subsidence and regional stress are higher on the eastern side than on the northern side. Hence, with increasing subsidence, the eastern part should fail prior to the northern side (Figures 10a and 10b). Combining regional extension and root subsidence reproduces well the observed lineaments on Alba Patera. On the contrary, the combination of regional stresses with surface loading augments the chance for strike-slip/normal faulting at the eastern foot of the volcano and by symmetry also at the western foot (Figure 10b). That means that surface loading combined with a regional extension is an unlikely process for creating localized concentric fractures on the upper and middle flanks of the volcano. This process is thus ruled out in the next sections.

[20] There is an asymmetry between the western and eastern flanks, i.e., confined and highly concentric Alba Fossae versus widespread and slightly concentric Tantalus Fossae (Figure 3) which can not be fully explained by an east-west regional stress for which the models are symmetric. We thus investigate a more complex regional stress field.

2.6. NW-SE Regional Stress With a S-N Decreasing Magnitude

[21] A greater distance to the Tharsis center should result in a decrease of the associated regional stress magnitude. Also the curvature of the observed fractures suggests different stress directions in the south and the north of Alba Patera (Figure 1a). We therefore approximate this pattern by a NW-SE regional extension with a south-north decrease of magnitude. On the eastern side,

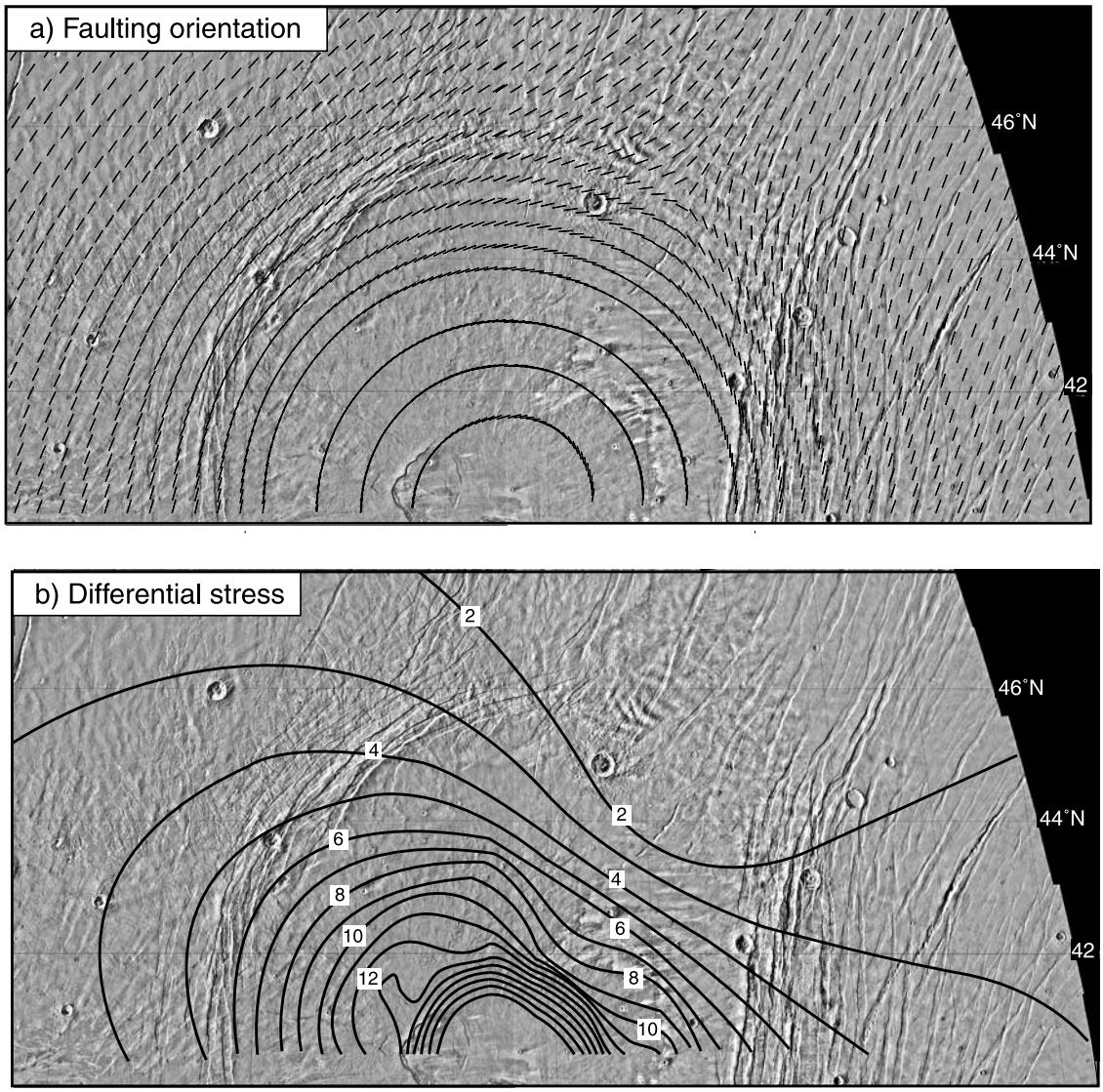

Figure 11. Subsidence due to a volcanic dense core with a NW–SE regional extension of S-N decreasing magnitude. a) The orientation of maximum compressive stress σ_1 gives the trends of faulting or dikes. b) The maximum differential stress ($\sigma_1 - \sigma_3$) in MPa indicates the position of likely failure. The core, whose density is 200 kg/m^3 higher, has a horizontal radius of 120 km and a vertical radius of 30 km. Depth to its top is 20 km. Without regional stress, the maximum tension has been found equal to 4 MPa, the maximum downward displacement 120 m. The regional extension varies from 2 MPa at 40° latitude to zero at 60° latitude. In order to compare the numerical results with the observed structures, the coordinates X, Y of the models have been changed in units from meters to degrees and from an aerocentric to an aerographic system (the planetographic system). The GMT plot is in a sinusoidal projection.

the predicted direction of normal faulting and dikes is concentric around the summit. Toward the eastern lower flanks of the volcano, this changes to a NE-SW linear trend similar to the Tantalus Fossae that parallel the eastern Catenae (Figure 11a). The Viking mosaic also shows a progression of Tantalus Fossae to a northeast direction toward the northern periphery in concordance with the models (Figure 3 and Figure 4d). On the western side, the predicted faulting is strongly concentric with a slight change toward the regional trend to the north. This reproduces the general pattern of Alba Fossae. Discrepancies between the orientation of maximum compressive stress or predicted faulting, and the observed tectonics are probably due to the reservoir shape and/or the regional stress of our models (see section 4).

[22] In addition, the calculation of differential stress indicating the position of likely failure provides important results (Figure 11b). On the northern side, the predicted orientation of faults does not correlate with the observed fault direction. These are older structures, however, which are unlikely to be reactivated by subsidence because it is situated in an area of low differential stress. The highest magnitudes of differential stress are obtained on the western flanks, inconsistent with a larger fractured area on the eastern flanks. Graben burial may be responsible for the apparent absence of concentric fractures on the mid-flanks

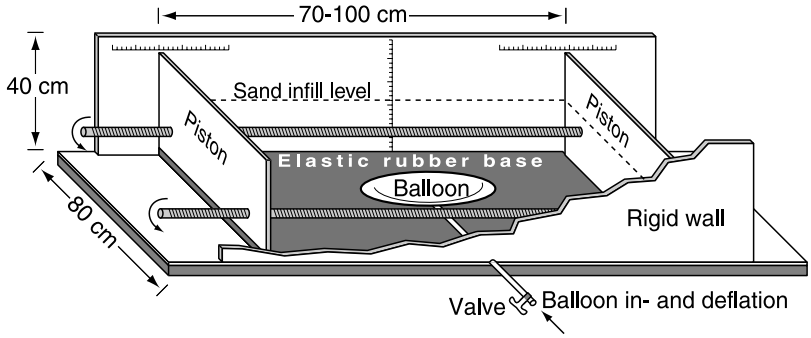

Figure 12. Experimental setup for physical sandbox models. The deformation rig was constructed in a way to superimpose homogeneous regional strain and local subsidence.

(Figure 4e). On the western lower flanks, regional Catenae display concentricity around Alba Patera similar to the structures on the upper flanks. This indicates the influence of the local field that could be well explained by the highest differential stress there. It has been proposed that Alba Fossae and Cyane Catenae belong to a unique system [*Mouginis-Mark et al.*, 1988; *Tanaka*, 1990]. A higher differential stress on the western flanks might promote dike intrusion into this flank and partly explain the 1 km rise in topography there compared to the eastern flank. The shape of Alba Patera, i.e., E-W elongated, could be also the consequence of such a localized stress concentration at the eastern and western flanks of the edifice (Figure 1b). On the summit, the NW-SE elongated contours of differential stress and the predicted compressive radial faulting (perpendicular to σ_1) correlate well with the wrinkle ridges on Alba Patera. Four branches of radial ridges are observed on the western side versus two branches on the eastern side and the whole set is NW-SE oriented (Figure 3).

[23] We have to make assumptions concerning the values of regional stress. The interplay between the regional and local stress allows us to assess realistic stress parameters. We discuss the maximum regional extension relative to the maximum local tensile stress. The regional stress is maximum at 40° latitude and decreases toward to the north. The local stress field, induced by the subsiding core alone, displays a maximum tensile stress at about 200–300 km radial distance from the axis of symmetry. The density difference between the core and surrounding rock is fixed at 200 kg/m^3. The influence of the stress values is best understood if different values are compared. a) A 4 MPa regional stress is suitable when the subsiding core has a horizontal radius in the upper limit defined in the tables of Figure 8. For example, for a core of 25 km vertical radius at 30 km depth, the horizontal radius is about 200–250 km. The maximum tensile stress due to core subsidence is then around 8 MPa. b) The regional stress is 2 MPa when the horizontal radius remains in the lower limit. The horizontal radius is now 150 km for a core of 25 km vertical radius at 30 km depth leading to a local maximum tension of about 4 MPa. c) For a high regional stress, e.g., 10 MPa, the core must extend excessively deep, beyond realistic crustal thickness. Hence the best fit is broadly found for the regional stress magnitude of about half the tension due to local subsidence.

[24] The above numerical models show that concentric faulting on the upper and mid-flanks of Alba Patera is best simulated when a volcanic core is shrinking and when simultaneously a regional NW-SE extension of S-N decreasing magnitude is present. The mechanism of subsidence is also tested in the physical models summarized in the following section.

3. Physical Models

3.1. Experimental Setup

[25] The aim of the sandbox models is to test physically the structural patterns caused by subsidence combined with regional extension. Physical models help to understand qualitatively geologic processes. They illustrate the effects of progressive deformation and showing a view of the structures that could arise on the surface [e.g., *Ramberg*, 1981]. The mechanism of local subsidence is simulated by a sill-shaped rubber balloon filled with air that may be deflated through a valve. Similar withdrawal experiments were performed for the purpose of understanding salt diapir migration, magma chamber withdrawal, and oil field exploitation [*Komuro et al.*, 1984; *Branney*, 1995; *Walter and Troll*, 2001]. We study the influence of circular and elliptic plan view forms of the balloon. The reservoir is placed in a sand box deformation rig similar to that used by *Cloos* [1930] for analogue experiments of extension in clay layers (Figure 12). The box is constructed to produce a regional linear extension. On the bottom of the box, an elastic layer is connected to two moving piston walls. Moving the walls away from each other stretches the bottom layer and transmits the extension to the overlying sand. The flat surface of the sand is covered by a fine layer of flour to visualize small-scale fractures.

[26] Since the physical models aim to reproduce natural-scale dimensions of the order of several hundreds of kilometers, geometric and mechanical scaling to smaller dimensions is necessary. We follow the classical scaling procedure from *Hubbert* [1937] and *Sanford* [1959]. To model in cm or dm size, the material properties must be of orders weaker than the prototype rocks. To obtain similar orientations of fractures, the internal friction coefficient of the analogue material is held constant. Moreover, to simulate natural rocks of cohesive strength between 10^6–10^7 Pa [*Schultz*, 1996] in laboratory scale,

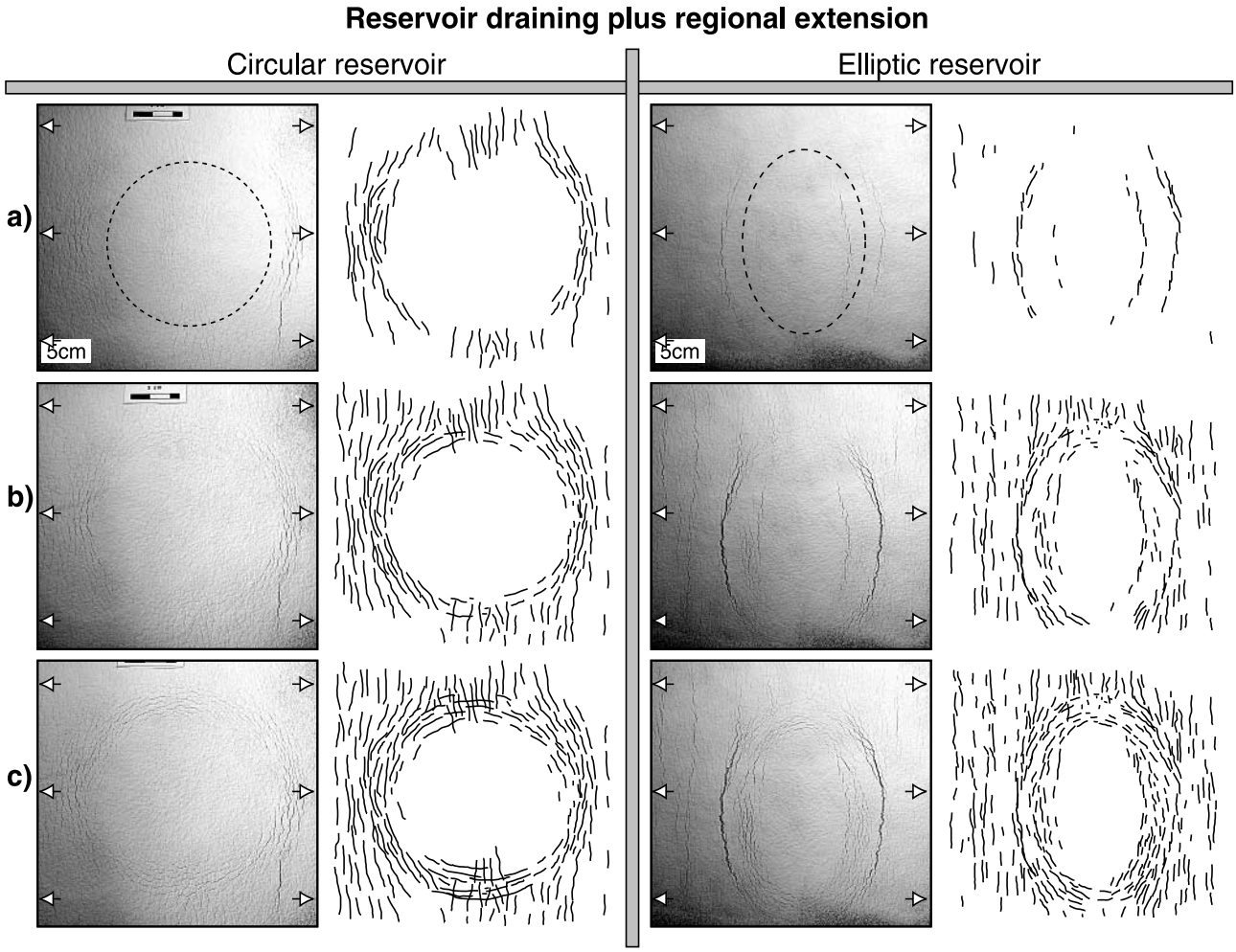

Figure 13. Physical models of reservoir draining plus regional extension. A circular (left) and elliptic (right) plan view shape of the balloon are tested. Note the changes from linear trends oriented N-S, to increasing concentricity with time.

low cohesive granular materials best fulfill mechanical scaling [*Ramberg*, 1981]. In previous analogue experimental studies, dry eolian sand was commonly used as analogue material, and mechanically tested for analogue scaling purposes [*Cobbold and Castro*, 1999]. We use a 0.4 mm grained quartz sand, for which the mechanical values are determined in direct shear tests. Cohesion of the used granular material is on the order of a few tens of Pascal, with a coefficient of internal friction of $\mu_s = 0.6$, obtaining fault inclinations of 33° relative to the maximum compressive principal stress σ_1. As in all physical models, some simplifications are necessary, e.g., the gravity acceleration is not scaled and the deflating balloon is considered as an approximation to any subsidence mechanism produced within a volcanic core. The regional extension of the sand box is measurable as a bulk horizontal widening per time unit. However, accurate values for Alba Patera are unknown. Prior to balloon contraction, a regional stress field is built up by 4% extension of the pistons. During balloon deflation, an overall bulk extension of 10% is chosen to be appropriate. Reservoir deformation and regional extension are simulated simultaneously. Surface deformations are measured and photographed, and afterward compared to the numerical models and the prototype Alba Patera.

3.2. Experimental Results

[27] In preliminary experiments without balloon deflation, normal faults develop perpendicular to the moving directions of the pistons. With the deflation of the balloon, two sequences of fracturing are observed on the surface. With increasing subsidence and regional extension, fracturing first appears following the modeled regional trend, i.e., mostly linear in north-south direction (Figure 13). Near the reservoir, surface fractures are concentric. New fracturing occurs in directions that are not favored by the regional stress field, transecting the linear structures. Multiple linear fractures form at the periphery. The regional stress affects the timing of fracture formation above the reservoir. It also modifies the correlation between the shape of the fracture set observed on the surface and the shape of the reservoir beneath. In experiments without regional extension, the concentric fractures outline approximately the shape and size of the balloon. An increase of horizontal extension causes a decrease of the correlation between the concentric fractures and the reservoir beneath. Extension stretches the

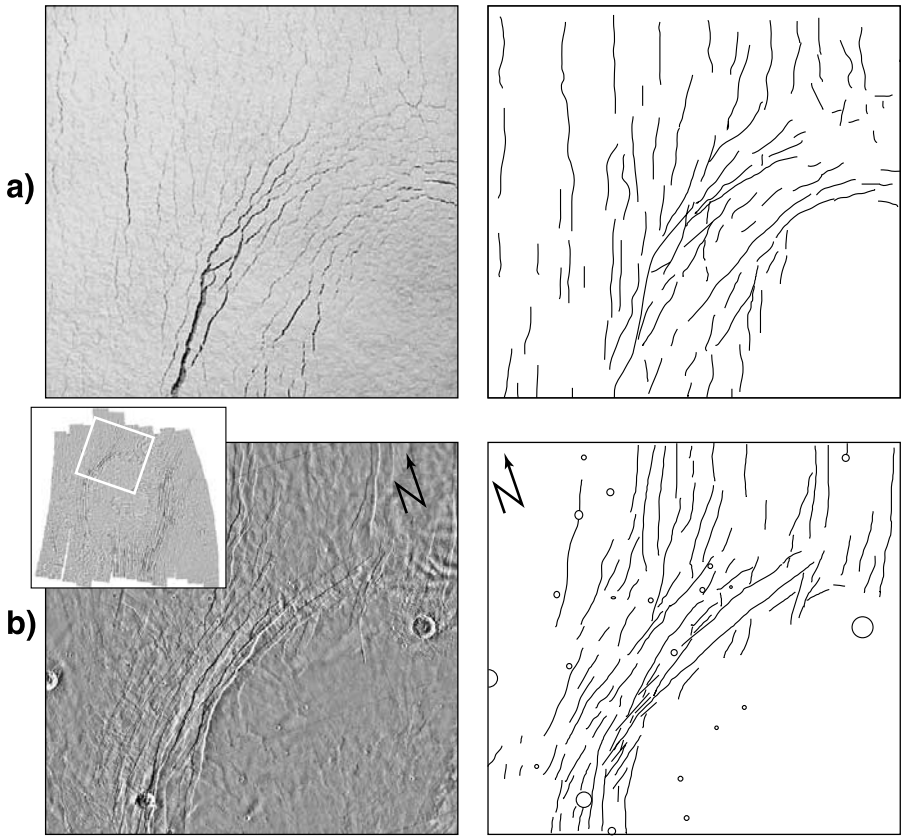

Figure 14. Subsidence a) simulated in physical models and b) observed on the northern part of Alba Fossae on the western side of Alba Patera.

fracture set in σ_3 direction, i.e., perpendicular to the moving walls. As a consequence, perfectly circular fractures in a tectonic environment can form only for an elliptic reservoir.

[28] The influence of the root size is herein illustrated by an elongated or circular balloon (Figure 13). Explicit concentricity is obtained all around the circular reservoir while the structures are more elongated for the deflation of an elliptic reservoir whose longer radius is perpendicular to the extension. For the oblong reservoir, two sets of concentric fractures are observed (Figure 13). The radius of the reservoir is situated within this range. The outer set is composed of unique long and large fractures which become deeper and wider with increasing subsidence. The characteristics of the set closer to the summit do not change, but new small and numerous similar fractures appear at further radial distances to join with the outer set of fractures.

[29] The analogue experiments provide important constraints about the tectonic evolution of Alba Patera, the shape of subsurface structure and the style of faulting. First, the two time sequences obtained with increasing subsidence correlate well with the observations on the northern side of Alba Fossae (Figure 14). The initial N-S oriented fractures that formed by ''regional extension'' are first captured by concentric fractures. There is continuity between concentric and linear structures. With ongoing balloon deflation, concentric fractures overprint the linear trend. Second, the type of faulting is ambiguous in numerical models when using Anderson's theory of faulting. Strike-slip faulting is predicted on the upper and mid-flanks while normal faulting or grabens are observed on Alba Patera. Analogue models show that the crust would likely fail in normal faulting rather than strike-slip faulting. Finally, concentricity is obtained well all around the circular balloon. An even better correlation is found with the deflation of the elliptic balloon which reproduces the north-south elongated set of concentric structures at Alba Patera.

4. Discussion

4.1. Models About Local and Regional Deformation

[30] Figure 15 summarizes the results of the numerical and analogue experiments. For the numerical models, some simplifications were necessary which need to be discussed. We prescribe axisymmetric models of subsidence. The shape of the subsurface structure could be completely defined in the future by the development of 3D numerical models. This would allow us to simulate the Tharsis stress field with a decreasing magnitude from Tharsis's center to its periphery and to change progressively the direction of fractures from radial to concentric and to improve the fit between predicted orientation of faults and observed structures (Figure 11a).

[31] We used an elastic half-space. In the presence of an underlying viscous mantle, mantle stresses relax with time, the support decreases and the local subsidence due to a dense crustal core is augmented. The local stresses within the elastic crust are thus expected to be greater. In such a case, the magnitude of added regional stresses would need

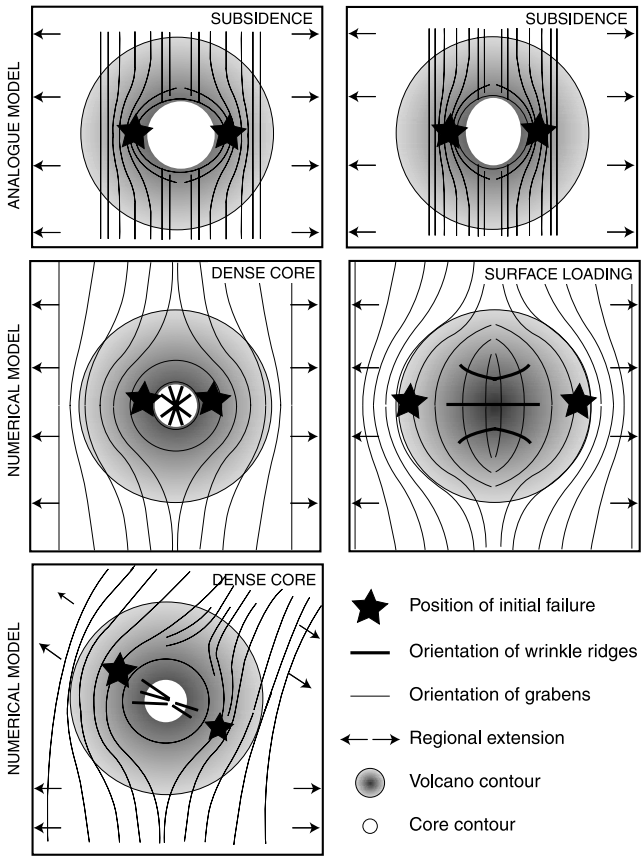

Figure 15. Summary of modeling results.

to be augmented. Moreover, the estimations of regional stress refer to the time of concentric graben formation. It is likely that the regional stress was not constant during Alba Patera's long-lived history. The regional stress field probably waned as shown by the change from the extended tectonic activity beyond Tharsis's rise in the early time of Tharsis history to confined activity at and around Tharsis Montes in its later stages [*Anderson et al.*, 2001]. The fact that younger concentric fractures on Alba Patera are more circular may be explained by decreasing regional extension or by increasing local subsidence.

[32] The models are performed with a flat plate. When the lateral size of a load is large compared to the radius of the planet, membrane stresses within a shell provide support to the load. *Turcotte et al.* [1981] inferred an approximate limit of 1300 km horizontal extent, i.e., 650 km radius, for the equal influence of bending and membrane stresses on Mars. The 100–200 km horizontal radius of the intrusive core is by far below this limit, so that the models of short-wavelength subsidence can be performed with a flat plate. The 650 km radius surface loading may be partially supported by membrane stresses. Planet curvature, however, does not change our contention that topographic loading is not responsible for graben formation on the upper and mid flanks of Alba Patera, for three reasons. 1) Planet curvature does not affect the wavelength of the deformation [*Freed et al.*, 2001]. The location of maximum tension due to partial bending is still situated at the foot of the volcano, implying that there is another mechanism for graben formation on Alba Patera. 2) Partial or total compensation by membrane stresses may induce concentric tension and radial grabens at the foot of the volcano. This does not correspond to the position and orientation of the concentric grabens. 3) With planet curvature, compression under the topographic load remains very high. Stresses due to topographic load must be negligible to observe tension on the upper and mid-flanks induced by a shrinking core (see combination of surface and subsurface loading in section 2.4 and Figure 9). The small influence of the long-wavelength and long-term topographic loading may be explained by a combination of membrane stresses and lithospheric viscous relaxation [*Zhong and Zuber*, 2000]. Finally, in numerical models that use Anderson's theory of faulting as their basis, strike-slip faulting is predicted instead of normal faulting (Figure 10a). The most probable explanation was proposed by *Freed et al.* [2001] who suggested that Anderson's theory of faulting does not take into account the regions of mixed-mode faulting. A combination of tectonic and magmatic stresses is suggested for the formation of particularly wide grabens on the flanks of Alba Patera [*Mège and Masson*, 1996]. In such a case, normal faulting would be facilitated by local extension above dike intrusions. Dikes follow the direction of minimum compressive stress and their orientations correlate well with the observed structures.

[33] In addition to the numerical models, physical models of subsidence lead to concentric structures similar to the observed grabens at Alba Patera. During the analogue experiments, linear fractures formed between the concentric fractures and the walls to the right and left sides (Figure 13). This may be explained by the setup of the experiments. Without a balloon, the "regional extension" simulated by the two moving piston walls was applied homogeneously on the whole surface. In reality, regional extension may be localized between about 100° and 118° longitude at Alba Patera regarding the occurrence of the regional western and eastern Catenae (Figure 3). This factor also applies to the numerical modeling. However, there is a progressive change from the concentric to the linear structures which are very similar to the eastern side of Alba Patera and are easily visible for the circular reservoir (Figure 13). On the western side, graben coverage seems to hinder the observation of such linear fractures. Another edge effect is the location of the balloon between the stretching elastic layer on the bottom and the surface, hindering the transmission of regional extension to the surface. No fracture occurs above the reservoir while faulting may be exaggerated above the edges of the reservoir between the zone without extension and the zone with extension. In reality, the frontier between compressive and tensile areas may vary relative to the size and depth of the reservoir and relative to the amount of regional extension as shown in the numerical modeling. However, this does not affect the two following results: 1) the elongation of the faulting relative to the horizontal reservoir shape, i.e., a circular reservoir gives an elliptic faulting pattern, 2) the timing of faulting, i.e., formation of concentric fractures parallel to the regional trend first, followed by concentric fractures perpendicular to the regional trend.

[34] Analogue and numerical results of a subsiding core give good correlation with concentric structures on Alba Patera. These complementary methods reproduce the struc-

tural geometric and evolutionary characteristics. The following discussion describes the possible mechanisms of subsidence specifically for the case of Alba Patera.

4.2. Origin of Root Subsidence

[35] Sinking crust can be caused by magma retreating from a magma chamber between eruptive stages or by increasing density during the cooling of magma or surrounding warm area [e.g., *Walker*, 1987, 1992; *Stofan et al.*, 1991]. Volcanic rift zones on ocean island volcanoes are thought to subside due to their incremental increase of density, restricted relative to the regions where less-dense eruptive products accumulate [*Walker*, 1992]. Solidifying magma bodies may contract and cause a density increase during crystallization and the release of gases [cf. *Tait et al.*, 1989]. Density changes within cooling magma bodies are typically within a range of 50–200 kg/m^3 [*Williams and McBirney*, 1979]. Cooling of an intrusion complex causes a significant volume decrease and thus increases the density in the core. This process is proposed to be realistic for Alba Patera because it was the locus of strong intrusive activity during giant dike swarm emplacement. Also, on Earth, the deep crustal roots of mountains may cause a local subsidence. An ageing orogenic root undergoes metamorphic reactions during long-term cooling resulting in a decrease in buoyancy [*Fischer*, 2002].

[36] Moreover, widespread distribution of the concentric grabens, from the upper to the mid-flanks of the volcano, indicates a vertical intrusion that forms the source of subsidence (Figure 7). Since the concentricity of the fractures becomes better pronounced with time, the influence of subsidence enhances incrementally within a period of order 1 Ga. A small vertical size of the high density core results in a short range of tensile stresses on the surface that necessitates a particularly large horizontal extent similar to the radial distance of the farthest grabens, up to 300 km. Neither such magma chamber size, nor similar longevity (1Ga) of chambers are known on Earth and therefore are not realistic. Magma chambers on Earth are active for just an instant if compared to the life span of a volcano [cf. *Marsh*, 2000]. Even long-lived magma reservoirs are active for time periods on the order of only a few ka. An intrusive core has been evidenced recently by short-wavelength gravity anomalies that do not correlate with the topography [*McGovern et al.*, 2001]. Accordingly, intrusive activity was an essential mechanism in the development of the volcanic field of Alba Patera.

[37] An alternative mechanism for the graben formation was proposed in which the relaxation of the topography induces tension on the upper flanks surrounded by compressive stresses [*Scott and Wilson*, 2003]. Compressive structures are, however, not present on the lower flanks nor on the surroundings of the volcano. Our models of subsidence, in contrast, predict compression on the summit area which may be in concordance with wrinkle ridges observed on the summit cone (Figure 3 and Figure 15). Cooling of an intrusive core could explain the absence of compressive structures on the flanks and also the increase of magma viscosity with time observed in the shortening of lava length [cf. *Schneeberger and Pieri*, 1991]. As proposed by *McGovern et al.* [2001], concentric normal faulting may be formed by sill complexes combined with a growing surface loading. These authors performed numerical models where upward pressures due to vertical displacements or density decrease are applied on elements at the same shallow initial depth and have identical values over a certain distance. These models show that a translation of the crust similar to the push of a piston occurs with horizontal deformation concentrated at the boundary of the reservoir (on the surface) and small deformation above it. The influence of topographic load on the flanks of the volcano was low compared to the subsurface forces. With this type of subsurface load, correlation of fractures with maximum stresses would therefore be found for a sill size approaching the radius of the observed fractures. Topographically, this corresponds to an upward translation and a notch on the flanks that was correlated by McGovern and co-authors to the flat zone surrounding the summit cone of Alba Patera (Figure 1b). For the piston scenario, the crust undergoes less deformation above the area of maximum external forces. This would also imply that the reservoir developed identical characteristics over 200–300 km radial distance corresponding to the locus of observed grabens, i.e., the stress field relations within the volcanic edifice must be remarkably homogeneous. A single or short event due to a piston-like deformation above a sill contrasts with the long-term incremental change from radial to concentric lineaments indicated by the structural study based on surface imaging.

4.3. A Geodynamic Model

[38] A comparison between the regions of faulting predicted by the modeling and the visual arrangement of lineaments observed on Alba Patera has been made in this study. Our physical and numerical experiments suggest that a regional stress field plus local subsidence were responsible for fracturing of the volcano. In order to understand the actual mechanism of regional and local deformation and to develop a geodynamic model, the long-term volcanic history must be considered.

[39] The early stage of Alba Patera is characterized by the formation of two radial branches of grabens (Figure 1). To the south, the Ceraunius Fossae are related to an east–west regional extension, radial to the Tharsis region. To the northeast, the Tantalus Fossae are interpreted as giant dike swarms injected from a magmatic center under Alba Patera [*Mège and Masson*, 1996; *Anderson et al.*, 2001]. On the basis of gravity anomalies, a plume model was proposed for Alba Patera [*Janle and Erkul*, 1991]. Coupled with the giant dike swarms, the widespread volcanism of the Alba Patera's earliest phase is comparable to flood basalt provinces commonly associated with hot spot and continental rifting episodes [*Richards et al.*, 1989; *Ernst et al.*, 2001], and represents the beginning stage of a billion-year active and centralized volcanic field. An issue is whether the Alba Patera hot spot rooted deep in the mantle as an individual plume or as a small blob of the Tharsis Plume, or instead was a consequence of crustal deformations and upper mantle decompression. In such context, local subsidence and concentric fractures during the middle stage of Alba Patera are coherent. An intrusive center and thermal subsidence are common features of hot spots, e.g., the vertical dike flows of the

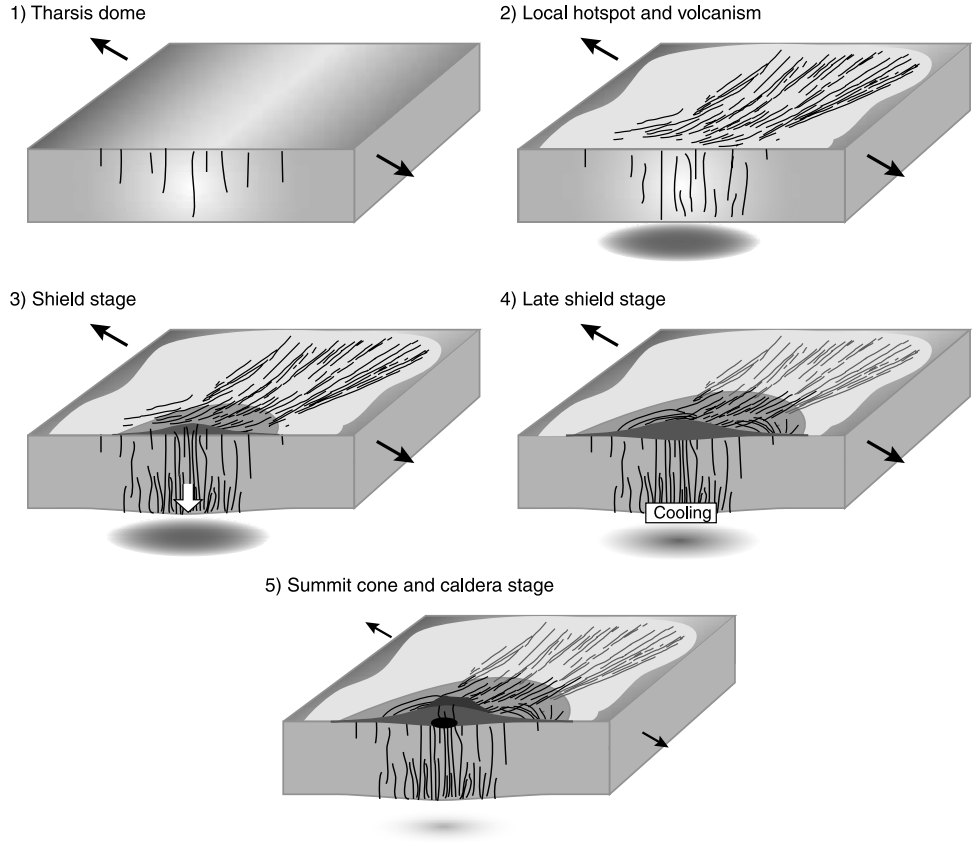

Figure 16. Geodynamic model of Alba Patera.

Muskox intrusion from the McKenzie plume, and the lithospheric cooling at the Snake River Plain of the Yellowstone hot spot [*Mège*, 2001].

[40] As studied on mosaic images, during the late stages of concentric fracturing the summit cone formed on Alba Patera (Figure 1b). The summit cone is characterized by a net increase of slope inclination compared to the underlying main shield which implies a higher viscosity, different magma composition and/or reduced feeding rates. On the basis of overlapping of fractures and lava flows, *Ivanov and Head* [2002] inferred a time relationship for the summit cone which formed during and after the concentric grabens. *Scott and Wilson* [2003] suggested that the summit cone is from a different magmatic source than the main shield, leading to its morphological change. Combined concentric and radial lineaments are observed on Earth, e.g., on the Galapagos Islands of Isabela and Fernandina [*McBirney and Williams*, 1969]. So-called overturned soup plate volcanoes, characterized by gently dipping lower flanks relatively steep upper flanks and a flat zone, are morphologically similar to Alba Patera. However, on the basis of crater counts and relative graben ages, the formation of circumferential lineaments on Alba Patera was established clearly in the later history of the volcanic shield. On the Galapagos volcanoes, concentric and radial dikes intrude synchronously or in multiple alternating stages [*Chadwick and Dieterich*, 1995]. Thus the mechanisms behind the inverted soup bowl volcano shapes are not adapted for Alba Patera. The conical shaped summit edifice in Alba Patera's latest stage does not indicate that a major fault reactivation occurred or that magma pathways were influenced by the circumferential fractures of the main shield. The large nested caldera depression, 140 km across on the top, shows that centralized shallow magma chamber(s) developed at the time of summit cone formation [*Mouginis-Mark and Rowland*, 2001; *Ivanov and Head*, 2002].

5. Summary and Conclusion

[41] As seen from the mosaic image analysis, the formation of circumferential grabens was increasingly pronounced toward the final stages of volcanic shield construction and was accompanied by a decrease of the volcanic feeding rate and an augmentation of the flank inclination with time. The concentric pattern that characterizes Alba Fossae and Tantalus Fossae on the mid and upper flanks of Alba Patera was reproduced by subsidence mechanisms using both physical and numerical methods. Continuity of these structures with radial-linear fractures indicates earlier phases when subsidence and regional extension were processes of similar magnitude. With ongoing subsidence, new fractures appeared with a pattern of increasing concentricity.

[42] A general understanding of the processes that gave rise to Alba Patera can be outlined from the forms of volcanism observed in relation to the tectonic structures

and from natural examples on the Earth (Figure 16). Flood basalts formed in the early stages; intrusions healed the widening crust during hot spot volcanism in the field of Alba Patera (stages 1 and 2). The root of the growing volcano was composed increasingly of intruded material, partly still parallel to the regional rift zone, but gradually more in a concentric fashion on the upper and mid-flanks of Alba Patera (stages 3 and 4). The mechanism of circular fracturing was not caused by short-time intrusive or tectonic activities but reflects a long-term mechanism active during several ten or even hundreds of millions years. This mechanism typically results from mantle derived intrusions or other mantle dynamic processes. A density increase of the mid and lower crust below Alba Patera probably formed a local stress field that was superposed on the regional tectonics and that was augmented with ongoing magmatic activity. The fact that the steep summit cone represents the final stage of a long volcanic evolution seems plausible in this dynamic concept.

[43] **Acknowledgments.** This paper benefited from thorough critics and suggestions by R. Ghent and an anonymous reviewer. Support was provided to B. Cailleau by the "Deutsche Forschungsgemeinschaft DFG" through a grant to the graduate school of Geomar - Kiel University "Dynamik global Kreisläufe im System Erde" (GRD171). T. Walter acknowledges a grant from the DFG (WA 1642). We would like to thank the MOLA science team for making many data freely available on the Web; herein we used MOLA images.

References

Anderson, E. M., *The Dynamics of Faulting and Dyke Formation With Applications to Britain*, 2nd ed., 206 pp., Oliver and Boyd, White Plains, N. Y., 1951.

Anderson, R. C., J. M. Dohm, M. P. Golombek, A. F. C. Haldemann, B. J. Franklin, K. L. Tanaka, J. Lias, and B. Peer, Primary centers and secondary concentrations of tectonic activity through time in the western hemisphere of Mars, *J. Geophys. Res.*, *106*, 20,563–20,585, 2001.

Banerdt, W. B., and M. P. Golombek, Tectonics of the Tharsis region of Mars: Insights from MGS topography and gravity, *Proc. Lunar. Planet. Sci. Conf. 31st*, abstract 2038, 2000.

Banerdt, W. B., M. P. Golombek, and K. L. Tanaka, Stress and tectonics on Mars, in *Mars*, edited by H. H. Kieffer et al., pp. 249–297, Univ. of Ariz. Press, Tucson, 1992.

Branney, M. J., Downsag and extension at calderas: New perspectives on collapse geometries from ice-melt, mining, and volcanoes, *Bull. Volcanol.*, *57*, 304–318, 1995.

Chadwick, W. W., and J. H. Dieterich, Mechanical modeling of circumferential and radial dike intrusion on Galapagos volcanoes, *J. Volcanol. Geothermal Res.*, *66*, 37–52, 1995.

Cloos, E., Künstliche Gebirge II, *Nat. Mus.*, *60*, 258–270, 1930.

Cobbold, P. R., and L. Castro, Fluid pressure and effective stress in sandbox models, *Tectonophysics*, *301*, 1–19, 1999.

Comer, R. P., S. C. Solomon, and J. W. Head, Mars: Thickness of the lithosphere from the tectonic response to volcanic loads, *Rev. Geophys.*, *23*, 61–92, 1985.

Ernst, R. E., E. B. Grosfils, and D. Mège, Giant dyke swarms: Earth, Venus and Mars, *Annu. Rev. Earth Planet. Sci.*, *29*, 489–534, 2001.

Fischer, K. M., Waning buoyancy in the crustal roots of old mountains, *Nature*, *417*, 933–936, 2002.

Freed, A. M., H. J. Melosh, and S. C. Solomon, Tectonics of mascon loading: Resolution of the strike-slip faulting paradox, *J. Geophys. Res.*, *106*, 20,602–20,620, 2001.

Gibbons, H. L., E. D. Scott, L. Wilson, and J. W. Head, Inferred properties of giant radial dikes beneath graben in northern Tharsis, *Proc. Lunar. Planet. Sci. Conf. 32nd*, abstract 1154, 2001.

Hartmann, W. K., and G. Neukum, Cratering chronology and evolution of Mars, in *Chronology and Evolution of Mars*, edited by R. Kallenbach et al., pp. 165–194, Kluwer Acad., Norwell, Mass., 2001.

Heller, A., and P. Janle, Lineament analysis and geophysical modelling of the Alba Patera Region on Mars, *Earth Moon Planets*, *84*, 1–22, 2000.

Hubbert, M. K., Theory of scale models as applied to the study of geologic structures, *Geol. Soc. Am. Bull.*, *48*, 1459–1520, 1937.

Ivanov, M. A., and J. W. Head, Alba Patera, Mars: Assessment of its evolution with MOLA and MOC data, *Proc. Lunar. Planet. Sci. Conf. 33rd*, abstract 1349, 2002.

Janle, P., and E. Erkul, Gravity studies of the Tharsis area on Mars, *Earth Moon Planets*, *53*, 217–232, 1991.

Komuro, H., Y. Fujita, and K. Kodama, Numerical and experimental models on the formation mechanism of collapse basins during the Green Tuff Orogenesis of Japan, *Bull. Volcanol.*, *47*, 649–666, 1984.

Marsh, B. D., Magma chambers, in *Encyclopedia of Volcanoes*, pp. 191–206, Academic, San Diego, Calif., 2000.

McBirney, A. R., and H. Williams, Geology and petrology of the Galapagos Islands, *Mem. Geol. Soc. Am.*, *118*, 197 pp., 1969.

McGovern, P. J., S. C. Solomon, J. W. Head, D. E. Smith, M. T. Zuber, and G. A. Neumann, Extension and uplift at Alba Patera: Insights from the MOLA observations and loading models, *J. Geophys. Res.*, *106*, 23,769–23,809, 2001.

Mège, D., Uniformitarian plume tectonics: The post-Archean Earth and Mars, in *Mantle Plumes: Their Identification Through Time*, edited by R. E. Ernst and K. L. Buchan, *Spec. Pap. Geol. Soc. Am.*, *352*, 141–164, 2001.

Mège, D., and P. Masson, A plume tectonics model for the Tharsis province, *Mars, Planet. Space Sci.*, *44*, 1499–1546, 1996.

Melosh, H. J., and A. Raefsky, Anelastic response of the Earth to a dip slip earthquake, *J. Geophys. Res.*, *88*, 515–526, 1983.

Mouginis-Mark, P. J., and S. K. Rowland, The geomorphology of planetary calderas, *Geomorphology*, *37*, 201–223, 2001.

Mouginis-Mark, P. J., L. Wilson, and J. R. Zimbelman, Polygenic eruptions on Alba Patera, *Bull. Volcanol.*, *50*, 361–379, 1988.

Ramberg, H., *Gravity, Deformation and the Earth's Crust in Theory, Experiments and Geological Applications*, 452 pp., Academic, San Diego, Calif., 1981.

Richards, M. A., R. A. Duncan, and V. E. Courtillot, Flood basalt and hot track: Plume heads and tails, *Science*, *246*, 103–107, 1989.

Sanford, A. L., Analytical and experimental study of simple geologic structures, *Bull. Geol. Soc. Am.*, *70*, 19–52, 1959.

Schneeberger, D. M., and D. C. Pieri, Geomorphology of Alba Patera, Mars, *J. Geophys. Res.*, *96*, 1907–1930, 1991.

Schultz, R. A., Relative scale and the strength and deformability of rock masses, *J. Struct. Geol.*, *18*, 1139–1149, 1996.

Scott, D. H., and K. L. Tanaka, Geologic map of the western equatorial region of Mars, scale 1:15,000,000, *U.S. Geol. Surv. Misc. Invest. Ser.*, *Map I-1802-A*, 1986.

Scott, E., and L. Wilson, Did the Alba Patera and Syria Planum regions of Mars lose their lithospheric roots in convective overturn events?, *J. Geophys. Res.*, *108*(E5), 5035, doi:10.1029/2002JE001492, 2003.

Scott, E. D., L. Wilson, and J. W. Head III, Emplacement of giant radial dikes in the northern Tharsis region of Mars, *J. Geophys. Res.*, *107*(E4), 5019, doi:10.1029/2000JE001431, 2002.

Sleep, N. H., and R. J. Phillips, Gravity and lithospheric stress on the terrestrial planets with emphasis on the Tharsis region of Mars, *J. Geophys. Res.*, *90*, 4469–4489, 1985.

Stofan, E. R., D. L. Bindschadler, J. W. Head, and E. M. Parmentier, Corona structures on Venus: Model of origin, *J. Geophys. Res.*, *96*, 20,933–20,946, 1991.

Tait, S., G. Wörner, P. V. D. Bogaard, and H. U. Schmincke, Cumulate nodules as evidence for convective fractionation in magma chambers, *J. Volcanol. Geotherm. Res.*, *37*, 21–37, 1989.

Tanaka, K. L., Tectonic history of the Alba Patera-Ceraunius Fossae region of Mars, *Proc. Lunar. Planet. Sci. Conf. 20th*, 515–523, 1990.

Tanaka, K. L., M. P. Golombek, and W. B. Banerdt, Reconciliation of stress and structural histories of the Tharsis region of Mars, *J. Geophys. Res.*, *96*, 15,617–15,633, 1991.

Turcotte, D. L., and G. Schubert, *Geodynamics: Applications of Continuum Physics to Geological Problems*, 450 pp., John Wiley, New York, 1982.

Turcotte, D. L., R. J. Willemann, W. F. Haxby, and J. Norberry, Role of membrane stresses in the support of planetary topography, *J. Geophys. Res.*, *86*, 3951–3959, 1981.

Turtle, E. P., and H. J. Melosh, Stress and flexural modeling of the Martian lithopsheric response to Alba Patera, *Icarus*, *126*, 197–211, 1997.

Twiss, R. J., and E. M. Moores, *Structural Geology*, 532 pp., W. H. Freeman, New York, 1992.

Van Wyk de Vries, B., and R. Matela, Styles of volcano-induced deformation: Numerical models of substratum flexure, spreading, and extrusion, *J. Volcanol. Geotherm. Res.*, *81*, 1–18, 1998.

Walker, G. P. L., The dike complex of Koolau Volcano, Oahu: Internal structure of a Hawaiian rift zone, in *Volcanism in Hawaii*, edited by R. W. Decker et al., *U.S. Geol. Surv. Prof. Pap.*, *1350*, 961–996, 1987.

Walker, G. P. L., "Coherent intrusive complexes" in large basaltic volcanoes—A new structural model, *J. Volcanol. Geotherm. Res.*, *50*, 41–54, 1992.

Walter, T. R., and V. R. Troll, Formation of caldera periphery faults, an experimental study, *Bull. Volcanol.*, *63*, 191–203, 2001.

Weijmars, R., *Principles of Rock Mechanics*, 360 pp., Alboran Sci., Amsterdam, Netherlands, 1997.

Williams, H., and A. R. McBirney, *Volcanology*, W. H. Freeman, New York, 1979.

Wilson, L., and J. W. Head III, Tharsis-radial graben systems as the surface manifestation of plume-related dike intrusion complexes: Models and implications, *J. Geophys. Res.*, *107*(E8), 5057, doi:10.1029/2001JE001593, 2002.

Wise, D. U., Faulting and stress trajectories near Alba Volcano, northern ridge of Mars, *Geol. Romana*, *15*, 430–433, 1976.

Zhong, S., and M. T. Zuber, Long-wavelength topographic relaxation for self-gravitating planets and implications for the time-dependent compensation of surface topography, *J. Geophys. Res.*, *105*, 4153–4164, 2000.

Zuber, M. T., The crust and mantle of Mars, *Nature*, *412*, 220–227, 2001.

B. Cailleau, GEOMAR, Wischhofstrasse 1-3, D-24148 Kiel, Germany. (bcaillea@geomar.de)

E. Hauber, Institut für Planetenforschung, Deutsches Zentrum für Luft- und Raumfahrt (DLR), Rutherfordstrasse 2, D-12489 Berlin, Germany. (ernst.hauber@dlr.de)

P. Janle, Institute of Geosciences, Department of Geophysics, Kiel University, Otto-Hahn-Platz 1, D-24118 Kiel, Germany. (pjanle@geophysik.uni-kiel.de)

T. R. Walter, Marine Geology and Geophysics, Rosenstiel School of Marine and Atmospheric Science, 4600 Rickenbacker Causeway, Miami, FL 33149, USA. (twalter@rsmas.miami.edu)